Chapter 3

Hybrid quantum-classical chaotic NEMS

3.1 Introduction

Classical or quantum finite systems may show non-deterministic behaviour when coupled to a stochastic bath (or other external randomness sources), or nonlinearity [209, 210]. In such hybrid systems any small perturbation destroys the regular motion and leads to unpredictable evolution of the system. In the first case, the stochasticity appears to be external, and in the second case, it is an intrinsic property of the system [211]. For example, in the case of a kicked rotator in classical regime, when the strength of kicking is increased, the regular periodic motion is destroyed and chaotic motion is observed. The chaotic behaviour can be validated by a diffusive growth in the kinetic energy [212, 213] of the kicked rotator. The quantum delta kicked rotators play an important role in understanding quantum chaos and other related effects [214]. The existence of quantum resonance can be seen using the quantum kicked rotators [215]. Experimentally the quantum kicked rotators and quantum chaos can be studied using ultracold atoms which are driven by periodically kicked by optical pulses [216]. The effect of the nonlinearity on a two-level system coupled with kicked rotor is already studied [217]. Dynamical chaos refers to the phenomenon of extreme sensitivity of phase trajectories to a tiny disturbance. It is worth to note that

in the quantum case, we do not have phase trajectories and the chaos is manifested in the Gaussian statistics of the energy spectrum [218]. The remarkable feature of quantum chaos is the termination of classically allowed diffusive processes leading to destruction of quantum coherence [219, 220]. In this chapter our interest is in a hybrid system under the constraint such that part of the system is classical, and the rest is quantum. In such a quantum-classical hybrid system when the classical part exhibits dynamical chaos, we analyze the spread of chaos to the quantum part. In the last few years the hybrid systems consisting of the spin and mechanical parts named as Nano-electromechanical systems (NEMS) generated a lot of interest [26, 27, 28, 29, 152, 153, 154, 155, 156, 157, 158, 159, 160, 161, 162, 163, 164, 165, 166, 167, 168, 169, 170, 171, 172, 173, 174]. In these systems the spin subsystem is always described quantum-mechanically and the mechanical subsystem (*i. e.*, the oscillator) can be considered either in quantum or classical (linear or nonlinear) regimes. All these cases need special mathematical description and show the realization of a physical features. Our interest here concerns the case when cantilever coupled to the NV center performs nonlinear oscillations. For more details about the model in question, we refer to the earlier works [168, 174, 221]. In particular, we assume that kicks of the external driving field force the classical motion of the cantilever and the overlapping of nonlinear resonances may induce the chaotic motion of the cantilever. The chaoticity of the motion of the cantilever extends to the quantum spin dynamics via the cantilever-spin coupling term. The spin of the NV center is described by spin triplet $S = 1$, with $m_s = -1,\ 0,$ and 1. States $|-1\rangle$ and $|1\rangle$ are separated by potential barrier $D\hat{S}_z^2 \approx \hbar\omega_0$, where $\omega_0 = 2.88$GHz. In what follows we set $\hbar = 1$. Hamiltonian of the NV center has the form [172]:

$$\hat{H}_{NV} = \sum_{i=\pm 1} \left(-\delta_i |i\rangle\langle i| + \frac{\Omega_i}{2}(|0\rangle\langle i| + |i\rangle\langle 0|) \right), \tag{3.1}$$

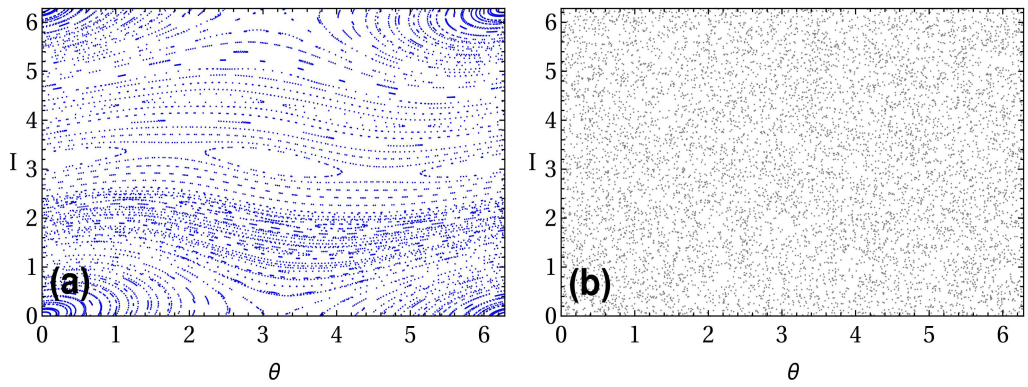

Fig. 3.1 The Phase space plot of cantilever's dynamics constructed through the recurrence relations Eq. (3.6) in (a) the regular regime $K = 0.5$ (Blue) where the phase space is covered by two different phase trajectories: open hyperbolic and some part of closed elliptic, and (b) the chaotic regime at $K = 10$ (Gray) where the entire phase space is covered by a chaotic sea. Topologically different phase trajectories are bordered by separatrix line. The values of parameters are: $K = \varepsilon I_0 T \frac{6\pi\mu}{m^2\omega_r^2}$, $\mu = \frac{\omega_r^2 m}{2a_0^2}$ $I_0 = \frac{m}{2}x_0^2\omega_r$, $m = 6\times10^{-17}$Kg, $x_0 = a_0 = 5\times10^{-3}$m, $T = 10\mu$s, $\omega_r = \omega_0 = 2\pi\times5\times10^6$Hz, for chaotic case $\varepsilon = 0.003$ and for the regular case $\varepsilon = 0.0003$.

where δ_i and Ω_i are detunings and Rabi frequencies of the two microwave (MW) transitions. In the limit of single MW field and zero external magnetic field $B_z \to 0$, Hamiltonian Eq.(3.1) couples the ground state $|0\rangle$ with bright superposition of the excited states $|b\rangle = (|-1\rangle + |1\rangle)/\sqrt{2}$, while dark state $|d\rangle = (|-1\rangle - |1\rangle)/\sqrt{2}$ is decoupled and NV center reduces to an effective two-level model. In what follows we consider both two- and three-level problems. In the case of coupling with the bright state the Hamiltonian of the hybrid system of NV center and a driven nonlinear oscillator is given as [173]

$$H\left(x,p,t\right) = H_S + H_0\left(x,p\right) + H_{NL} + \varepsilon V\left(x,t\right) + g\hat{V}_{c,NV}. \tag{3.2}$$

Here $\hat{H}_S = \frac{1}{2}\omega_0\hat{\sigma}_z$ is the Hamiltonian of the NV center, The splitting frequency is given by $\omega_0 = \left(\omega_R^2 + \delta^2\right)^{1/2}$, where ω_R is the Rabi frequency, and δ is the detuning. The spin operator $\hat{S}_{z,NV}$ can be written in the basis of NV center as [173]: $\hat{S}_{z,NV} = \frac{1}{2}\big(\cos(\alpha)\hat{\sigma}_z + \sin(\alpha)(\hat{\sigma}_+ + \hat{\sigma}_-)\big)$ with $\tan(\alpha) = -\omega_R/\delta$ and $\hat{\sigma}_z = |e\rangle\langle e| - |g\rangle\langle g|$, $\hat{\sigma}_+ = |e\rangle\langle g|$, $\hat{\sigma}_- = |g\rangle\langle e|$. The linear part of the oscillator is given by term $H_0 = \frac{p^2}{2m} + \frac{\omega_r^2 m x^2}{2}$ and the nonlinear

part is given by $H_{NL} = \beta x^3 + \mu x^4$, where ω_r is the frequency of the oscillations, β and μ are constants of the nonlinear terms. The term

$$V(x,t) = V_0 xT \sum_{n=-\infty}^{\infty} \delta(t - nT),$$
$$\varepsilon V_0 = f_0, \quad \varepsilon \ll 1, \tag{3.3}$$

describes the driven motion of the cantilever in the microwave field of delta pulses with frequency $\omega = 2\pi/T$. The key issue is the last term $\hat{V}_{c,NV} = x(t)\hat{S}_{z,NV}$ in Eq. (3.2) which describes the coupling between the classical cantilever and the quantum NV spin. The distance and the coupling strength between the magnetic tip and NV spin depend on the magnetostriction effect [174]. Subject to the cantilever's oscillations, $x(t)$ can be either chaotic or regular. In what follows, we show that classical dynamical chaos leads to the stochastic phenomenon in spin dynamics. We consider two and three level models of the NV center and show that in both cases chaotic dynamics of the cantilever leads to the chaotic spin dynamics. However, being stochastic, two-level model does not manifest all the characteristic features of quantum chaos. In the present chapter our main focus is a mathematical formulation of the problem. Nevertheless, we specify the values of the parameters relevant to the NV centers [172]: $\frac{\omega_r}{2\pi} = 5$ MHz, $\frac{\omega_R}{2\pi} = 0.1 - 10$ MHz, $\delta = 1$ kHz, mass of the cantilever $m = 6 \times 10^{-17}$ kg, the coupling constant $\frac{g}{2\pi} = 100$ kHz, the amplitude of the zero point fluctuations $a_0 = \sqrt{\hbar/2m\omega_r} \approx 5 \times 10^{-3}$ m. The nonlinear constants are order of $\beta \approx \frac{\omega_r^2 m}{2a_0}$, $\mu \approx \frac{\omega_r^2 m}{2a_0^2}$. The energy scale of the problem is defined by $\varepsilon V \approx \omega_r^2 m a_0^2 \approx 10^{-9}$J, and the time scale is of order of microsecond scale $t \approx \frac{\pi}{2g}$ microseconds. In what follows, we explore the spreading of classical dynamical chaos on the quantum system. In the quantum part of the NEMS, spin dynamics manifest some characteristic features of the quantum chaos [94, 186, 188, 189], but not all of them. Therefore, we term this phenomenon as a hybrid quantum-classical chaos. The work is organized as follows: In section 3.2, we discuss the classical chaotic dynamics of the

cantilever. In section 3.3, we present analytical results for spin dynamics of NV center spin attached to the cantilever and discuss different aspects of the quantum chaos, namely, quantum coherence, Poincaré recurrences and level statistics. Subsequently in section 3.4 we study dynamics of a three-level NV system. Later, in section 3.5 we explore statistical average over various I_0 and θ_0. In section 3.6 we study about feedback effect and finally summarize the manuscript in section 3.7.

3.2 Dynamics of the cantilever

The experimentally feasible NEMS consists of the spin of the NV center interacting with a magnetic tip (attached to the end of the nano-cantilever). The oscillations performed by the cantilever can be viewed as classical or quantum, depending on the simple criteria: At temperatures $T << 2\pi\hbar\omega_r/k_B$, where k_B is the Boltzmann constant and ω_r is the oscillation frequency, dynamics of a cantilever is quantum, and it exerts quantum feedback effect on a spin dynamics. Typically for $\omega_r = 1$kHz, $T < 50$nK. At higher temperatures, or when the cantilever is controlled externally by a classical field, dynamics is classical. Large-amplitude nonlinear oscillations are entirely classical. Therefore in what follows, we neglect the quantum feedback effect.

With the purpose of simplicity, the cantilever part of the Hamiltonian $H_{p,q} = H_0 + H_{NL} + V(x,t)$ can be rewritten in the action-angle canonical variables through the transformation $\Phi = F + I\theta$:

$$d\Phi = pdq + \theta dI + \left(H_{I,\theta} - H_{p,q}\right)dt. \tag{3.4}$$

The canonical equations in the new variables are given as

$$\begin{aligned}\frac{dI}{dt} &= -\frac{\partial H_{I,\theta}}{\partial \theta} = -\varepsilon \frac{\partial V(I,\theta)}{\partial \theta} T \sum_{n=-\infty}^{\infty} \delta(t-nT), \\ \frac{d\theta}{dt} &= \frac{\partial H_{I,\theta}}{\partial I} = \omega(I) + \varepsilon \frac{\partial V(I,\theta)}{\partial I} T \sum_{n=-\infty}^{\infty} \delta(t-nT).\end{aligned} \tag{3.5}$$

The presence of the delta function allows us to introduce the Floquet map $(I_{n+1}, \theta_{n+1}) = \mathscr{F}(I_n, \theta_n)$ and integrate Eq. (3.5) exactly as

$$\begin{aligned}I_{n+1} &= I_n - \varepsilon T \frac{\partial V(I_n,\theta_n)}{\partial \theta_n}, \\ \theta_{n+1} &= \theta_n + \omega(I_{n+1})T + \varepsilon T \frac{\partial V(I_n,\theta_n)}{\partial I}.\end{aligned} \tag{3.6}$$

From the above equation we deduce the criteria of the dynamical chaos:

$$K = \varepsilon I_0 T \left| \frac{d\omega(I)}{dI} \right|, \tag{3.7}$$

Using action-angle variable to transform the cantilever part of the Hamiltonian $H_{p,q} = H_0 + H_{NL} + V(x,t)$, and taking average with respect to the fast phase θ, the cubic part of H_{NL} will be zero if we take average with respect to fast phase θ but the quartic term in H_{NL} will survive, so we obtain, from here $\omega(I) = \partial(H_0 + H_{NL})/\partial I$, $H_0(I) = \omega_r I + H_{NL}$, $H_{NL} = 3\pi\mu \left(\frac{I}{m\omega_r}\right)^2$, and $V = V_0(I)\cos\theta$, $V_0(I) = V_0\sqrt{2I_0/\omega_r}$. Using the system specific parameters we define the criterion for dynamical chaos as:

$$K = \varepsilon I_0 T \left(\frac{6\pi\mu}{m^2\omega_r^2}\right). \tag{3.8}$$

K is also known as a criterion for overlapping of the resonance. If $K < 1$ the phase trajectories are distinguishable from each other and if $K > 1$ phase trajectories correspond to chaotic behaviour [186].

After the formation of dynamical chaos, the dynamical description of the problem loses the sense. The dynamics of the cantilever can be explored using a standard map $I_{n+1} = I_n - K\sin\theta_n$, $\theta_{n+1} = \theta_n + I_{n+1}$, where K quantifies the criterion for the dynamical chaos. For further analytic insights, we utilize the methods of non-equilibrium statistical physics and introduce the distribution function $f(\theta, I)$ such that $i\frac{\partial f}{\partial t} = \left(\hat{L}_0 + \varepsilon\hat{L}_1\right)$, where Liouville operators $\hat{L}_0$ and $\hat{L}_1$ are defined as follows (see [186] for more details) $\hat{L}_0 = -i\omega\frac{\partial}{\partial\theta}$, and $\hat{L}_1 = -i\left(\frac{\partial V}{\partial I}\frac{\partial}{\partial\theta} - \frac{\partial V}{\partial\theta}\frac{\partial}{\partial I}\right)$. The critical issue is the difference between the time scales of the slow action I and fast angle θ variables. The correlation time scale in the system is defined via $\langle\langle\theta(t)\theta(0)\rangle\rangle = \exp(-t/\tau_c)$. Typically $\tau_c < T < \tau_D$, where τ_D is the time spent on the substantial change of the action variable. As we see from Eq. (3.5), during the interval between the kicks T, the change of the action variable is small and is proportional to ε. Our interest here concerns the distribution function for the action variable, and the Fokker-Plank equation averaged over the fast angular variable $F(I) = \langle\langle f(I,\theta)\rangle\rangle_\theta$. The general structure of the Fokker-Planck equation reads [186]:

$$\frac{\partial F(I)}{\partial t} = -\frac{\partial}{\partial I}(A(I)F(I)) + \frac{1}{2}\frac{\partial^2}{\partial I^2}(B(I)F(I)), \tag{3.9}$$

where $A = \frac{1}{T}\langle\langle\Delta I\rangle\rangle_\theta$, and $B = \frac{1}{T}\langle\langle(\Delta I)^2\rangle\rangle_\theta$. After calculating coefficients explicitly, we deduce the kinetic equation as

$$\frac{\partial F}{\partial t} = \tfrac{1}{2}\tfrac{\partial}{\partial I}D(I)\tfrac{\partial F}{\partial I}, \tag{3.10}$$

where $D(I) = \pi\varepsilon^2\sum\limits_{m,p} m^2|V_m|^2\delta(m\omega - p\Omega)$, $\Omega = 2\pi/T$, V_m is the Fourier component of the interaction term and m, p indices take into account the multiple internal resonances. The solution of the kinetic equation reads as

$$\langle I(t)\rangle = I_0^2 + Dt,\ D = \frac{1}{2}\varepsilon V^2 T, \tag{3.11}$$

where D is the diffusion coefficient. The dynamics of the cantilever is chaotic for $K > 1$ and otherwise $K < 1$ is regular (see Fig. 3.1). In the chaotic regime we observe a sea of phase points uniformly distributed over the phase space. In the regular regime, two different phase space trajectories cover the entire space. For the standard map described above, if the parameter $K > K_c = 0.9716$, the stochastic layers start merging; thus, it will create a domain of chaotic motion that covers whole phase space. As K increases, the islands' size decreases, and only the largest of them can be found in the chaotic sea. Thus solution for cantilever can be written in the discrete form $x_n = \sqrt{2I_n/m\omega_r}\cos\theta_n$, $p_n = -\sqrt{2I_n\omega_r m}\sin\theta_n$.

3.3 Spin-1/2 system attached to the cantilever

3.3.1 Evolved in time wave function

Let us consider a hybrid system of Quantum NV spin attached to a classical cantilever whose dynamics is calculated from a standard map. From the Hamiltonian given by Eq. (3.2) we see that the effect of the cantilever in the NV spin is due the the interaction term $\hat{V}_{c,NV}$. Therefore, the effective Hamiltonian of the NV center attached to the cantilever can be written as:

$$\hat{H}_n = \frac{1}{2}\omega_0\hat{\sigma}_z + g\hat{V}_{c,NV}, \tag{3.12}$$

where $\hat{V}_{c,NV} = \sqrt{2I_n/m\omega_r}\cos\theta_n\hat{S}_{z,NV}$. It is important to note here that I_n and θ_n follow the Floquet map given by Eq. (3.6). By varying the parameter K we change the characteristic of the term $\hat{V}_{c,NV}$ from the regular to the chaotic dynamics of the cantilever and explore the spin dynamics in both cases. Exploiting the Floquet theory [222] we solve the Schrödinger

equation analytically and get the state after time $t = NT$ as

$$|\psi(t = NT)\rangle = \hat{\mathscr{U}}^N |\psi(0)\rangle, \tag{3.13}$$

where $\hat{\mathscr{U}}^N$ is the time evolution operator evolving the system after N kicks and $|\psi(0)\rangle$ is the initial state of the system. The Floquet map $\hat{F}_n$ after the n^{th} kick is $\hat{\mathscr{F}}_n = \exp\left(-i\hat{H}_n T\right)$ and the evolution operator $\hat{\mathscr{U}}^N$ is a time-ordered product of $\hat{\mathscr{F}}_n^s$ given as $\hat{\mathscr{U}}^N$ $= \hat{\mathscr{F}}_N \cdots \hat{\mathscr{F}}_{n+1} \hat{\mathscr{F}}_n \hat{\mathscr{F}}_{n-1} \cdots \hat{\mathscr{F}}_3 \hat{\mathscr{F}}_2 \hat{\mathscr{F}}_1$. The exact wave function after time $t = NT$ can be written in the form

$$|\psi(t = NT)\rangle = \sum_{\{\alpha_n\}=\pm} \left\{ \prod_{n=2}^{N} e^{-i\alpha_n \varphi_n} \left\langle \varphi_n^{\alpha_n} \middle| \varphi_{n-1}^{\alpha_{n-1}} \right\rangle \right\} e^{-i\alpha_1 \varphi_1} \left\langle \varphi_1^{\alpha_1} \middle| \psi(0) \right\rangle \left| \varphi_N^{\alpha_N} \right\rangle. \tag{3.14}$$

Here $\alpha_n \varphi_n$ and $|\varphi_n^{\alpha_n}\rangle$ ($\alpha_n = \pm$) are the eigenvalues and eigenstates, respectively of the nth Floquet operator $\hat{\mathscr{F}}_n$.

The general form of the eigenstates is quite involved (not shown). However, in the resonant limit $\tan(\alpha) = -\omega_R/\delta \gg 1$, we can simplify the Floquet map $\hat{\mathscr{F}}_n$. The spectral decomposition of $\hat{\mathscr{F}}_n$ is given as

$$\hat{\mathscr{F}}_n = \exp\{-i\varphi_n\} |\varphi_n^+\rangle\langle\varphi_n^+| + \exp\{i\varphi_n\} |\varphi_n^-\rangle\langle\varphi_n^-|. \tag{3.15}$$

Here the quasienergy φ_n is given by $\varphi_n = \frac{(\sqrt{\chi_n^2 + \omega_0^2})T}{2}$, where we introduced the notation $\chi_n = g\sqrt{2I_n/m\omega_r}\cos\theta_n$. The normalized eigenstates are $|\varphi_n^+\rangle = \eta_n|0\rangle + \xi_n|1\rangle$, and $|\varphi_n^-\rangle = \xi_n|0\rangle - \eta_n|1\rangle$, where $\eta_n = \frac{k_n}{\sqrt{1+k_n^2}}$, $\xi_n = \frac{1}{\sqrt{1+k_n^2}}$, and $k_n = \frac{\omega_0 + \sqrt{\chi_n^2 + \omega_0^2}}{\chi_n}$. Now let us consider that initially the system is prepared in the state $|\psi(0)\rangle = |0\rangle$. Therefore, the

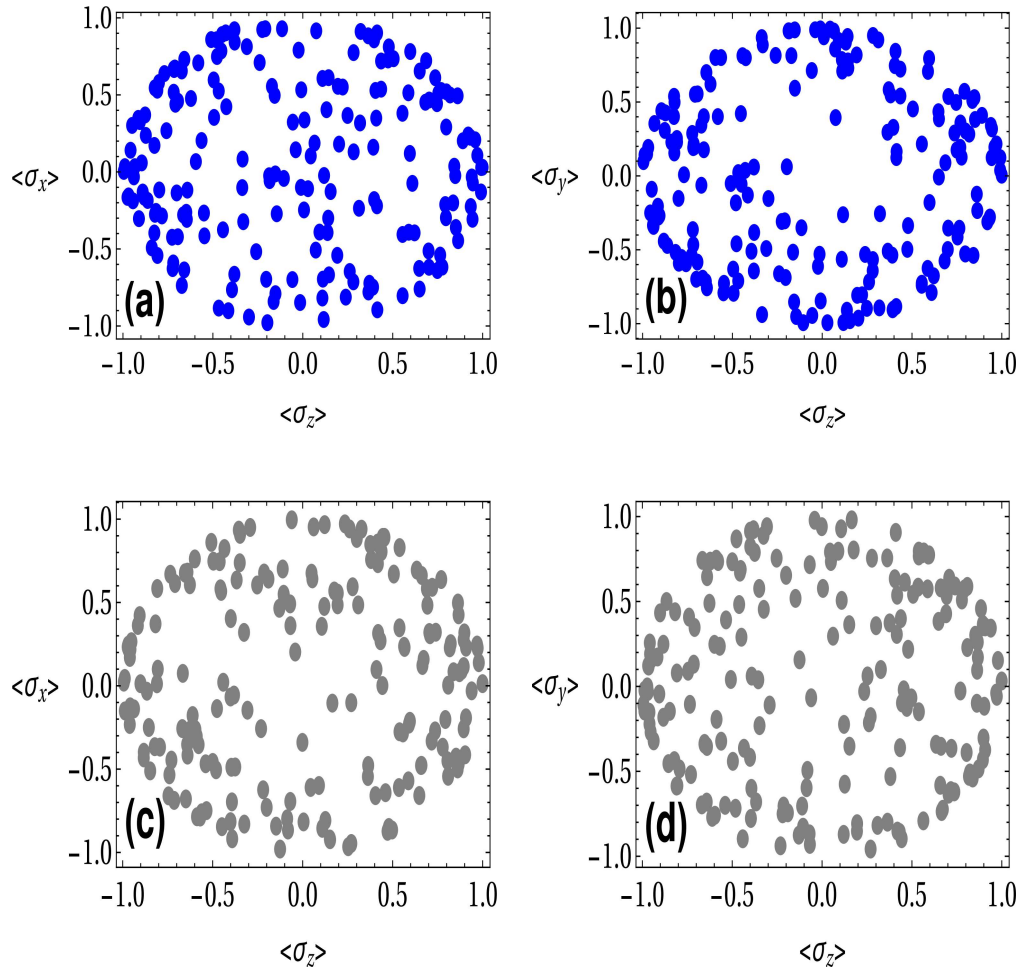

Fig. 3.2 Poincaré sections for $(\langle\sigma_x\rangle,\ \langle\sigma_z\rangle)$ and $(\langle\sigma_y\rangle,\ \langle\sigma_z\rangle)$ in the regular regime at $K = 0.5$ ((a) and (b)) and chaotic regime at $K = 10$ ((c) and (d)) . The parameters are $m = 1$, $g = 1$, $\omega_0 = 1$, $\omega_r = 0.2$, $T = 1$, $\alpha = \pi/2$. The values of the parameters in the real units are $K = \varepsilon I_0 T \frac{6\pi\mu}{m^2\omega_r^2}$, $\mu = \frac{\omega_r^2 m}{2a_0^2}$, $I_0 = \frac{m}{2}x_0^2\omega_r$, $m = 6\times10^{-17}$Kg, $x_0 = a_0 = 5\times10^{-3}$m, $T = 10\mu$s, $\omega_r = \omega_0 = 2\pi\times5\times10^6$Hz, for chaotic case $\varepsilon = 0.003$ and for the regular case $\varepsilon = 0.0003$.

explicit form of the evolved wave function is calculated as

$$
\begin{aligned}
&|\psi(t=NT)\rangle = \mathscr{A}_{11}\{\eta_1\exp(-i\varphi_1)(\eta_N|0\rangle+\xi_N|1\rangle)\}+\mathscr{A}_{12}\{\eta_1\exp(-i\varphi_1)(\xi_N|0\rangle\\
&-\eta_N|1\rangle)\}+\mathscr{A}_{21}\{\xi_1\exp(i\varphi_1)(\eta_N|0\rangle+\xi_N|1\rangle)\}+\mathscr{A}_{22}\{\xi_1\exp(i\varphi_1)(\xi_N|0\rangle-\eta_N|1\rangle)\},\\
&\mathscr{A} = \prod_{n=2}^{N} G_n\{\varphi\},\\
&G_n\{\varphi\} = \begin{bmatrix} \exp(-i\varphi_n)(\eta_n\eta_{n-1}+\xi_n\xi_{n-1}) & \exp(-i\varphi_n)(\eta_n\xi_{n-1}-\xi_n\eta_{n-1}) \\ \exp(i\varphi_n)(\xi_n\eta_{n-1}-\eta_n\xi_{n-1}) & \exp(i\varphi_n)(\eta_n\eta_{n-1}+\xi_n\xi_{n-1}) \end{bmatrix}.
\end{aligned}
\tag{3.16}
$$

For more details of the analytical solution and normalization of the wave function, we refer to Appendix B . S-I and Appendix B . S-II. Taking into account Eq. (3.14) - Eq. (3.16) we calculate the expectation values of the spin components $\langle\sigma_\alpha\rangle$, $\alpha = x,y,z$. The explicit formulas are given in the Appendix B . S-III.

We note that $\varphi_n = \frac{(\sqrt{\chi_n^2+\omega_0^2})T}{2}$, where $\chi_n = g\sqrt{2I_n/m\omega_r}\cos\theta_n$ and $(I_n,\ \theta_n)$ is described by the map Eq. (3.6). Therefore, depending on the parameter of stochasticity K, the phase φ_n can be either non-commensurate and random or smooth and regular. In the spirit of the work [223] we explore the interplay between the chaotic classical (cantilever) and quantum (NV spin) dynamics in the next section.

3.3.2 Expectation values of the NV spin components

We see from Fig. (3.1) that the Poincaré sections for $(I_n,\ \theta_n)$ clearly distinguish the motion of cantilever in the regular and chaotic regime. Now if we attach a NV center spin to the cantilever, we need to check whether the Poincare sections of the spin dynamics show a contrast in the regular and chaotic regimes of the cantilever or not. For this purpose we plot the Poincaré section of $(\langle\sigma_x\rangle,\ \langle\sigma_z\rangle)$ and $(\langle\sigma_y\rangle,\ \langle\sigma_z\rangle)$ in Fig. 3.2(a) and (b) when cantilever performs motion in regular regime and (c) and (d) when cantilever performs motion in chaotic regime. We fail to distinguish the effects due to regular and chaotic regions in the Poincaré sections of the spin dynamics of the NV center.

The Poincaré sections of the spin dynamics evolve more or less in the same manner for both the regular and the chaotic cases (see Fig. 3.2). In order to delve deeper to identify the differences, we calculate the Fourier power spectrum for observances defined as $I_{x,y,z} = \left| \int_{-\infty}^{\infty} \langle\sigma_{x,y,z}\rangle \exp(-i\omega t)dt \right|^2$. The Fourier power spectrum as shown in Fig. 3.3 displays differences in the regular and chaotic regime. We see that when stochasticity parameter varies from $K = 0.5$ (regular) to $K = 10$ (chaotic), the broadness of power spectrum increases. It is much broader in the chaotic case as compared to the regular case.

The broadening of spectrum is a signature of chaos which sets in our system for $K > 1$. We see that the Fourier spectra of all spin components $\langle\sigma_{x,y,z}\rangle$, are broadened. To see the behavior of spin dynamics, we plot the time dependence of different spin components. While $\langle\sigma_{x,y,z}\rangle$ components perform fast, chaotic oscillations in chaotic regime (see Figs. 3.4 (b), (d) and (f)), they show quasi-periodic oscillation in the regular regime (see Figs. 3.4 (a), (c) and (e)).

3.3.3 Quantum coherence

Quantum coherence is the resource for performing vast number of quantum information protocols. In many-body system the quantum coherence is the essence of entanglement and plays an important role in understanding some physical phenomena of quantum information and quantum optics. Relative entropy and l1-norm measures are also a monotone of coherence [202]. By incoherent operations one can generate coherence that quantifies maximal entanglement [224]. The loss of coherence in a quantum system may happen due to two different reasons: In one case when the system is in contact with the environment or a thermal bath, the coupling to the environment may cause decoherence, which is a stochastic phenomenon. In the other case, the coupling of a quantum system with a classical chaotic system, may lead to a loss of coherence. We focus on the second case where dynamical chaos due to the non-linearity in the classical system [225] may result a loss of coherence. Here we explore the problem of generation of coherence for the NV spin coupled to a nanocantilever in a regular or a chaotic regime.

In particular, we prepare the NV center initially in a mixed state:

$$\hat{\rho}(0) \quad = \quad p_1|0\rangle\langle 0| + p_2|1\rangle\langle 1|. \tag{3.17}$$

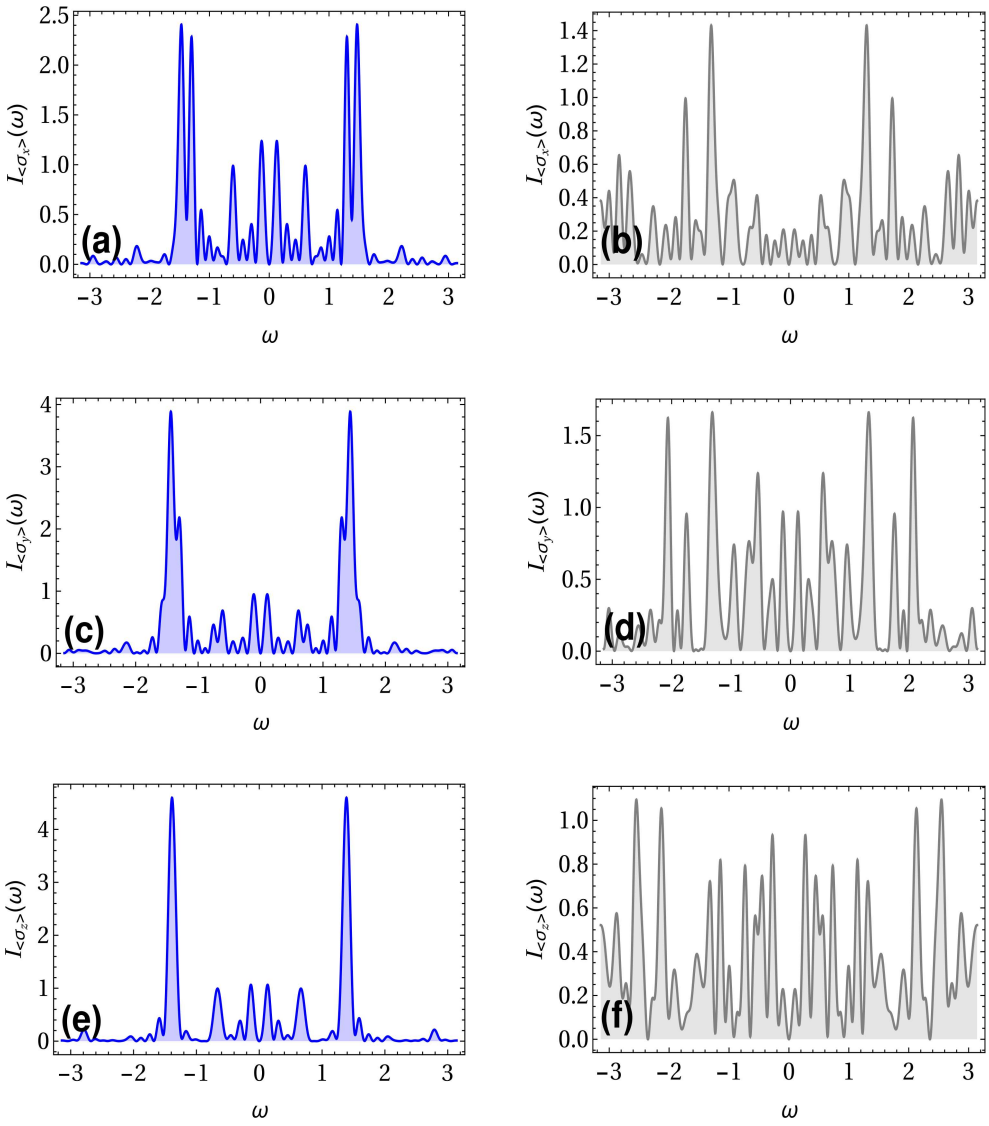

Fig. 3.3 Fourier Power spectrum density for expectation values of $\sigma_{x,y,z}$ in the regular regime ((a), (c) and (e)) at $K = 0.5$ (Blue), and in the chaotic regime ((b), (d) and (f)) at $K = 10$ (Gray). The parameters used for the plot are $m = 1$, $g = 1$, $\omega_0 = 1$, $\omega_r = 0.2$, $T = 1$, $\alpha = \pi/2$. The values of the parameters in the real units: $K = \varepsilon I_0 T \frac{6\pi\mu}{m^2\omega_r^2}$, $\mu = \frac{\omega_r^2 m}{2a_0^2}$ $I_0 = \frac{m}{2}x_0^2\omega_r$, $m = 6\times10^{-17}$Kg, $x_0 = a_0 = 5\times10^{-3}$m, $T = 10\mu$s, $\omega_r = \omega_0 = 2\pi\times5\times10^6$Hz, for chaotic case $\varepsilon = 0.003$ and for the regular case $\varepsilon = 0.0003$.

The time evolved density matrix is given by evolution operator Eq. (3.13) as:

$$\hat{\rho}(t) = (\hat{\mathscr{U}}^N)^{-1}\hat{\rho}(0)\hat{\mathscr{U}}^N, \tag{3.18}$$

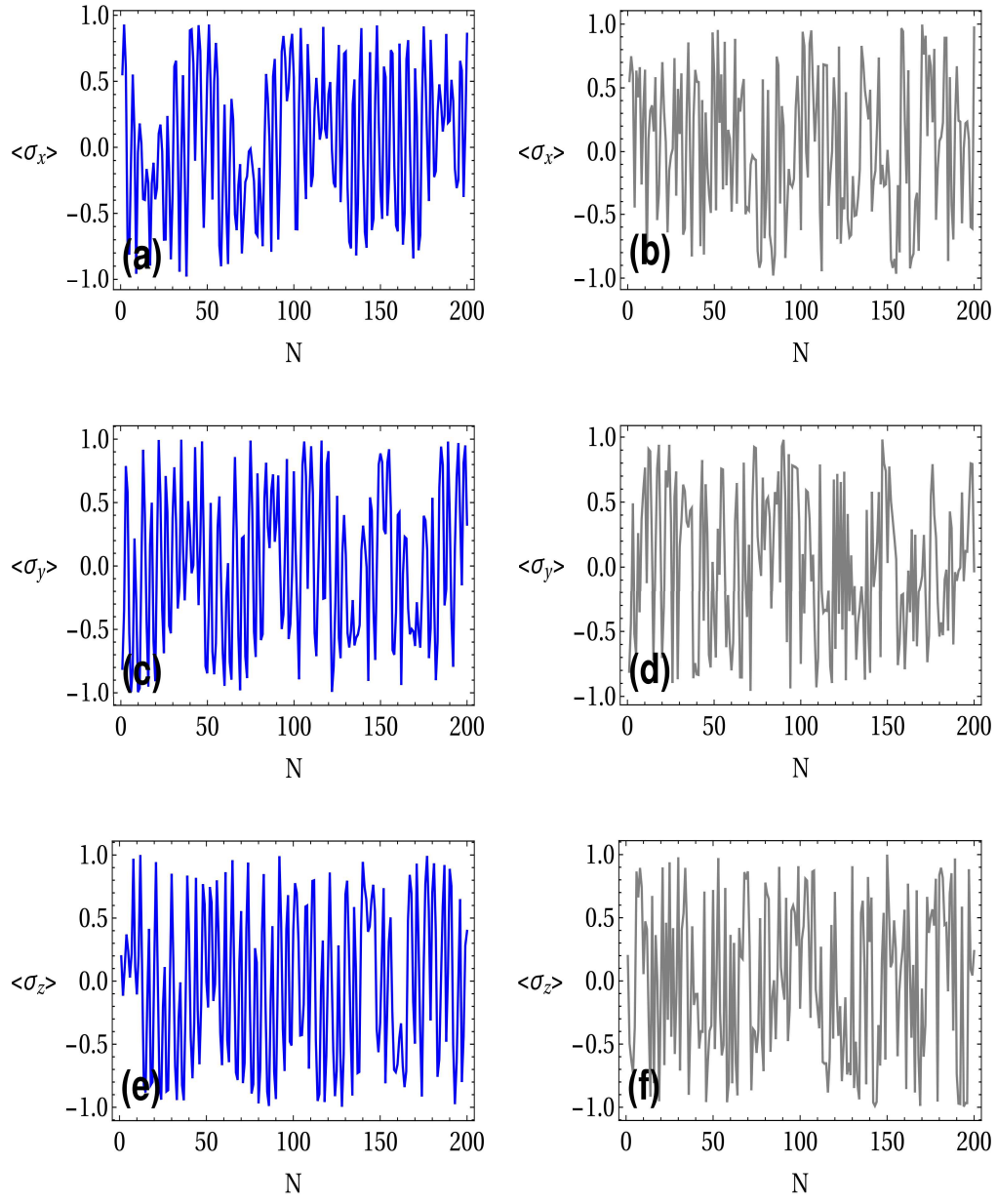

Fig. 3.4 Spin dynamics for $\langle\sigma_x\rangle$, $\langle\sigma_y\rangle$ and $\langle\sigma_z\rangle$ in the regular regime at $K = 0.5$ (see (a), (c) and (e)) and $\langle\sigma_x\rangle$, $\langle\sigma_y\rangle$ and $\langle\sigma_z\rangle$ in the chaotic regime at $K = 10$ (see (b), (d) and (f)). The parameters are $m = 1$, $g = 1$, $\omega_0 = 1$, $\omega_r = 0.2$, $T = 1$, $\alpha = \pi/2$. The values of the parameters in the real units: $K = \varepsilon I_0 T \frac{6\pi\mu}{m^2\omega_r^2}$, $\mu = \frac{\omega_r^2 m}{2a_0^2}$, $I_0 = \frac{m}{2}x_0^2\omega_r$, $m = 6\times10^{-17}$Kg, $x_0 = a_0 = 5\times10^{-3}$m, $T = 10\mu$s, $\omega_r = \omega_0 = 2\pi\times5\times10^6$Hz, for chaotic $\varepsilon = 0.003$ and for regular $\varepsilon = 0.0003$.

$$\hat{\rho}(t) = \rho_{11}|0\rangle\langle 0| + \rho_{12}|0\rangle\langle 1| + \rho_{21}|1\rangle\langle 0| + \rho_{22}|1\rangle\langle 1|. \tag{3.19}$$

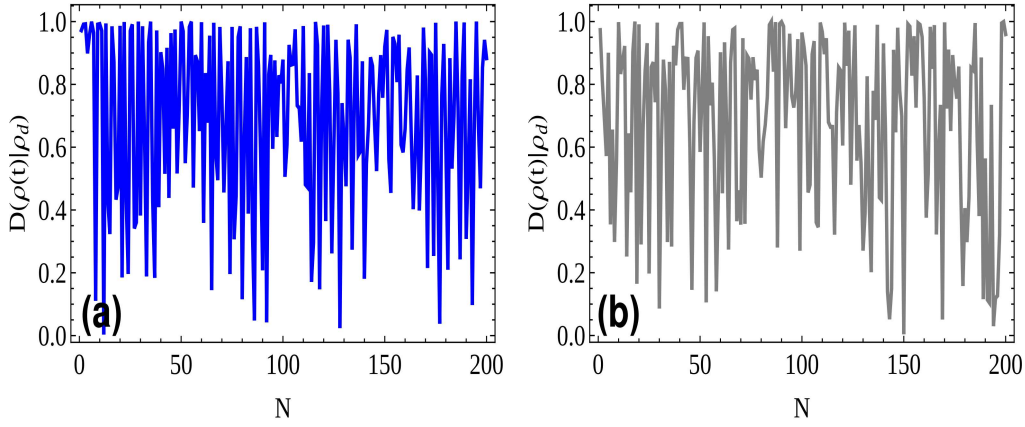

Fig. 3.5 The quantum coherence in (a) the regular regime at $K = 0.5$ (Blue) and (b) the chaotic regime at $K = 10$ (Gray), for the following values of the parameters $m = 1, g = 1$, $\omega_0 = 1$, $\omega_r = 0.2$, $T = 1$, $\alpha = \pi/2$. The values of parameters are $K = \varepsilon I_0 T \frac{6\pi\mu}{m^2\omega_r^2}$, $\mu = \frac{\omega_r^2 m}{2a_0^2}$ $I_0 = \frac{m}{2}x_0^2\omega_r$, $m = 6\times10^{-17}$Kg, $x_0 = a_0 = 5\times10^{-3}$m, T=10$\mu$s, $\omega_r = \omega_0 = 2\pi\times5\times10^6$Hz, for chaotic $\varepsilon = 0.003$ and for regular $\varepsilon = 0.0003$.

The elements of the time-evolved density matrix are given in the Appendix B . S-IV, where all the elements of $\hat{\rho}(t)$ are time-dependent. We quantify the quantum coherence in terms of the relative entropy as

$$\mathscr{D}\big(\hat{\rho}(t)|\hat{\rho}_d(t)\big) = Tr\{\hat{\rho}(t)\ln\hat{\rho}(t) - \hat{\rho}(t)\ln\hat{\rho}_d(t)\}. \tag{3.20}$$

Here $\hat{\rho}_d(t)$ is the diagonal part of $\hat{\rho}(t)$. The eigenvalues of the density matrix $\rho(t)$ are: $E_\pm = \frac{1}{2}\Big(\rho_{11}+\rho_{22}\pm\sqrt{\rho_{11}^2+\rho_{22}^2+4\rho_{21}\rho_{12}-2\rho_{11}\rho_{22}}\Big)$. Now, taking into account Eq. (3.16), we calculate quantum coherence in terms of relative entropy as:

$$\mathscr{D}\big(\hat{\rho}(t)|\hat{\rho}_d(t)\big) = E_+\ln E_+ + E_-\ln E_- - \rho_{11}\ln\rho_{11} - \rho_{22}\ln\rho_{22}. \tag{3.21}$$

The stochasticity parameter K appears in the expression of $\rho(t)$ as η_N, ξ_N which contain I_n and θ_n. The relative entropy $\mathscr{D}$ for regular and chaotic cases are plotted in Fig. 3.5. We see that quantum coherence in regular case is doing quasi-periodic oscillation while in chaotic regime coherence varies abruptly. This observation supports the fact that the chaos destroys the quantum coherence.

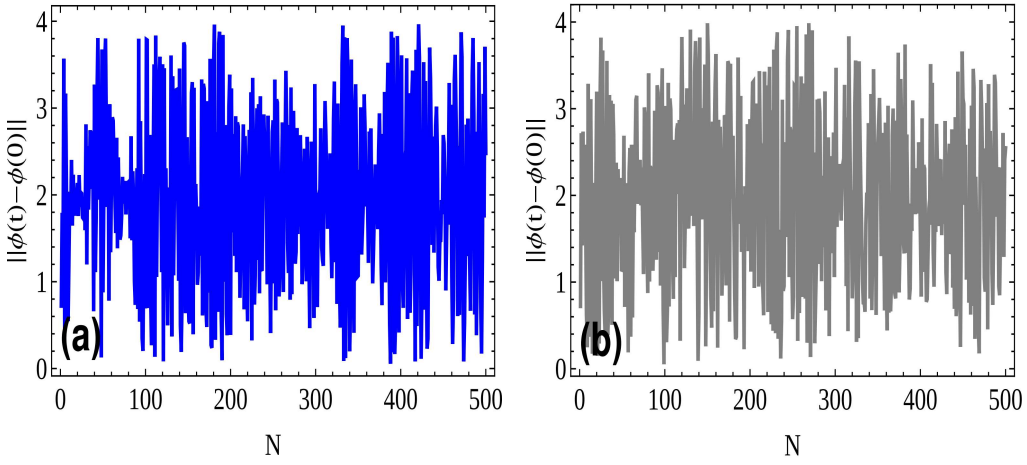

Fig. 3.6 Quantum Poincaré recurrence as a function of time (*i.e.*, number of kicks) in (a) the regular regime at $K = 0.5$ (Blue) and (b) the chaotic regime at $K = 10$ (Gray). The parameters are $m = 1$, $g = 1$, $\omega_0 = 1$, $\omega_r = 0.2$, $T = 1$, $\alpha = \pi/2$. The values of parameters: $K = \varepsilon I_0 T \frac{6\pi\mu}{m^2\omega_r^2}$, $\mu = \frac{\omega_r^2 m}{2a_0^2}$ $I_0 = \frac{m}{2}x_0^2\omega_r$, $m = 6\times10^{-17}$Kg, $x_0 = a_0 = 5\times10^{-3}$m, T=10$\mu$s, $\omega_r = \omega_0 = 2\pi\times5\times10^6$Hz, for chaotic $\varepsilon = 0.003$ and for regular $\varepsilon = 0.0003$.

3.3.4 Quantum Poincaré recurrence

"Any phase-space configuration (I,θ) of a system enclosed in a finite volume will be repeated as accurately as one wishes after a finite interval of time". This statement is the essence of the Poincaré recurrence theorem and holds in the quantum case also [226]. Any time-dependent periodic Hamiltonian would reunite itself infinitely often over time. Suppose the system has a continuous energy spectrum corresponding to the classical systems, then the quantum recurrence theorem does not hold. A quantum system that is bounded defined by a Hamiltonian H_0 has a discrete spectrum when subjected to a nonresonant time-dependent periodic potential V with $V(t) = V(t+\tau)$ for an arbitrary period τ. For any initial configuration of the system, both the wave function and the energy reunite itself over time [227]. The time passed off during the recurrence is known as Poincaré recurrence time. The Quantum Poincaré recurrence means that the distance between the initial and evolved states can become smaller than the characteristic ε: $\|\phi(t) - \phi(0)\| < \varepsilon$. Taking Eq. (3.16) into account the explicit expression for the distance of the

time evolved state from the initial state is:

$$\|\phi(t)-\phi(0)\| = 2-\Big(A_{11}^{*}\eta_1^{*}\exp(i\varphi_1)\eta_N^{*}+A_{12}^{*}\eta_1^{*}\exp(i\varphi_1)\xi_N^{*}+ A_{21}^{*}\xi_1^{*}\exp(-i\varphi_1)\eta_N^{*}+A_{22}^{*}\xi_1^{*}\exp(-i\varphi_1)\xi_N^{*}+A_{11}\eta_1\exp(-i\varphi_1)\eta_N +A_{12}\eta_1\exp(-i\varphi_1)\xi_N+A_{21}\xi_1\exp(i\varphi_1)\eta_N+A_{22}\exp(i\varphi_1)\xi_N\Big). \tag{3.22}$$

The above expression of quantum Poincaré recurrences is plotted for the regular $K<1$ and chaotic cases $K>1$ separately in Fig. 3.6 (a) and (b), respectively. From these figures we see a slight difference in behavior of the system in two regimes. In the regular case Fig. 3.6 (a) we see a trend of quasiperiodic modulation of the amplitude, while in the chaotic case Fig. 3.6 (b), the distance measure between the wave functions is the essence of a noise. Analyses of the recurrence show the absence of the exponential decay of Poincaré recurrence, while the exponential decay is a hallmark of quantum chaos [228]. The effect we observe in our system is non-conventional for quantum chaos. The reason for the absence of the conventional quantum chaos phenomenon is the low dimensionality of the spin space. On the other hand, chaotic dynamics of cantilever plays the role of external noise for NV spin and has a stochastic character rather than a dynamical. It destroys the nature of quasiperiodic revivals in spin dynamics, and quantum recurrence becomes a random event. The dynamics of the quantum system is distinct from the behavior of the regular systems. Therefore, we term this effect as hybrid quantum-classical chaos.

One of the interesting characteristics of the hybrid quantum-classical chaos is the time-translation symmetry breaking (TTSB). The Hamiltonian $\hat{H}_n$ Eq. (3.12), taken at different times form a set of noncommuting Hamiltonians: $\hat{H}_n$. The integer n defines discrete moment of time $t_n = nT$, where T is the period between the pulses applied to the cantilever. Therefore, $\hat{H}_n$ is a set of elements repeated in time $\hat{H}_n(I_n\,\theta_n) \equiv \hat{H}_{n+k}(I_{n+k},\,\theta_{n+k})$, when canonical variables repeat their values $(I_{n+k},\,\theta_{n+k}) = (I_n,\,\theta_n)$ *i.e.*, the Floquet time crystal [229, 230]. On the other hand the quantum Poincaré recurrence occurs if the distance

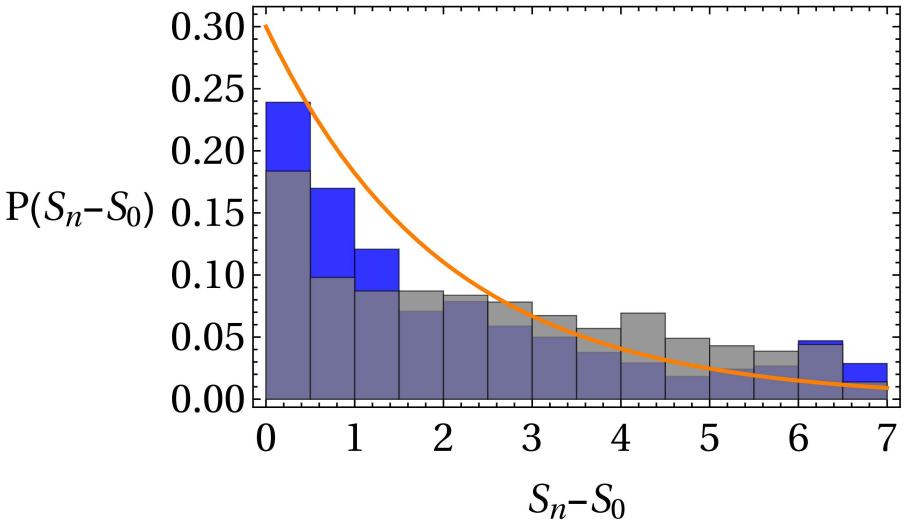

Fig. 3.7 Histogram plot of level statistics of Hamiltonian $\hat{H}_n$ in the regular regime at $K = 0.5$ (Blue) and in the chaotic regime $K = 10$ (Gray). A reference plot for poissonian statistics (Orange) is also shown. For this plot we have taken upto 1000 kicks to get the ensemble. The parameters are $m = 1$, $g = 1$, $\omega_0 = 1$, $\omega_r = 0.2$, T=1, $\alpha = \pi/2$. The values of parameters: $K = \varepsilon I_0 T \frac{6\pi\mu}{m^2\omega_0^2}$, $\mu = \frac{\omega_r^2 m}{2a_0^2}$ $I_0 = \frac{m}{2}x_0^2\omega_r$, $m = 6\times10^{-17}$Kg, $x_0 = a_0 = 5\times10^{-3}$m, T=10$\mu$s, $\omega_r = \omega_0 = 2\pi\times5\times10^6$Hz, for chaotic case $\varepsilon = 0.003$ and for the regular case $\varepsilon = 0.0003$.

between state vectors is small $\|\phi((n+k)T) - \phi(nT)\| < \varepsilon$, where ε is the characteristic small parameter of the recurrence. The time-translation symmetry underlies conservation of energy, reproducibility of the wave function and Hamiltonian. TTSB occurs if for each t_n and for every state $|\phi(nT)\rangle$ there exists an operator $\mathscr{A}$ for which at least one of the two conditions $\hat{H}_n(I_n, \theta_n) \equiv \hat{H}_{n+k}(I_{n+k}, \theta_{n+k})$ and $\langle|\phi(nT)|\mathscr{A}||\phi(nT)\rangle = \langle|\phi((n+k)T)|\mathscr{A}||\phi((n+k)T)\rangle$ is violated. In our case operator $\mathscr{A}$ corresponds to the spin operator $\mathscr{A} \equiv \hat{S}$. We note that the conditions $\hat{H}_n(I_n, \theta_n) \equiv \hat{H}_{n+k}(I_{n+k}, \theta_{n+k})$, and $(I_{n+k}, \theta_{n+k}) = (I_n, \theta_n)$ hold only in the regular case (elliptic trajectories) and are violated in the chaotic case when invariant torus are destroyed and dynamics is not periodic in the phase space. TTSB occurs due to the hybrid character of quantum classical chaos, meaning that Quantum Poincaré recurrence of the wave function holds while the periodicity of the Hamiltonian not.

3.3.5 Level statistics for spin-1/2 case

The eigenvalues of the the Hamiltonian $\hat{H}_n$ (Eq. (3.12)) are given by: $E^{(n)}_{1,2} = \pm\frac{1}{2}\sqrt{\chi_n^2 + \omega_0^2}$, where $\chi_n = g\sqrt{\frac{2I_n}{m\omega_0}}\cos\theta_n$. Each Hamiltonian from the set $\{\hat{H}_n\}$ has two energy levels. We explore the distances between the levels:

$$S_n = E^{(n)}_1 - E^{(n)}_2 = \sqrt{\omega_0^2 + g^2\Big(\frac{2I_n}{m\omega_0}\Big)\cos^2\theta_n}, \tag{3.23}$$

for each Hamiltonian and construct the distribution functions $P(S_n - S_0)$ for regular $K < 1$ and chaotic $K > 1$ cases. Here S_n is the separation between two energy levels and S_0 corresponds to the maximum of $P(S_0)$. We see that the level statistics is Poissonian in the both regular $K < 1$ and chaotic $K > 1$ cases. Comparing results of spin dynamics Figs. 3.3 and 3.4, with level statistics Fig. 3.7 we see that in the both cases level statistics is of Poissonian type, while we expect it to be Gaussian in chaotic case [231]. Thus for spin 1/2 case, in spite of the chaotic quantum spin dynamics we do not observe statistical characteristics of quantum chaos.

3.4 Dynamics of a three-level NV system

We proceed to analyse a more general case and consider a three-level NV center. The effective Hamiltonian of the NV center for spin $S = 1$ attached to the cantilever can be written as:

$$\hat{H}_n = \hat{H}_{NV} + g\hat{V}_{c,NV}, \tag{3.24}$$

where $\hat{H}_{NV} = \sum\limits_{i=\pm1}\Big(-\delta_i|i\rangle\langle i| + \frac{\Omega_i}{2}(|0\rangle\langle i| + |i\rangle\langle 0|)\Big)$ is the Hamiltonian of the NV center [172] and $\hat{V}_{c,NV} = \sqrt{2I_n/m\omega_r}\cos\theta_n\hat{S}_{z,NV}$ is the coupling term with the nonlinear cantilever. For spin $S = 1$, $S_{z,NV} = \frac{1}{2}(\cos\alpha S_z + \sin\alpha S_x)$, where $S_{x,z} = \sigma_{x,z}(1)$ is spin components for $S = 1$ case. For numerical calculations we consider $\delta_{\pm1} = \delta = 1$ and $\Omega_\pm = \Omega = 1$. Similar

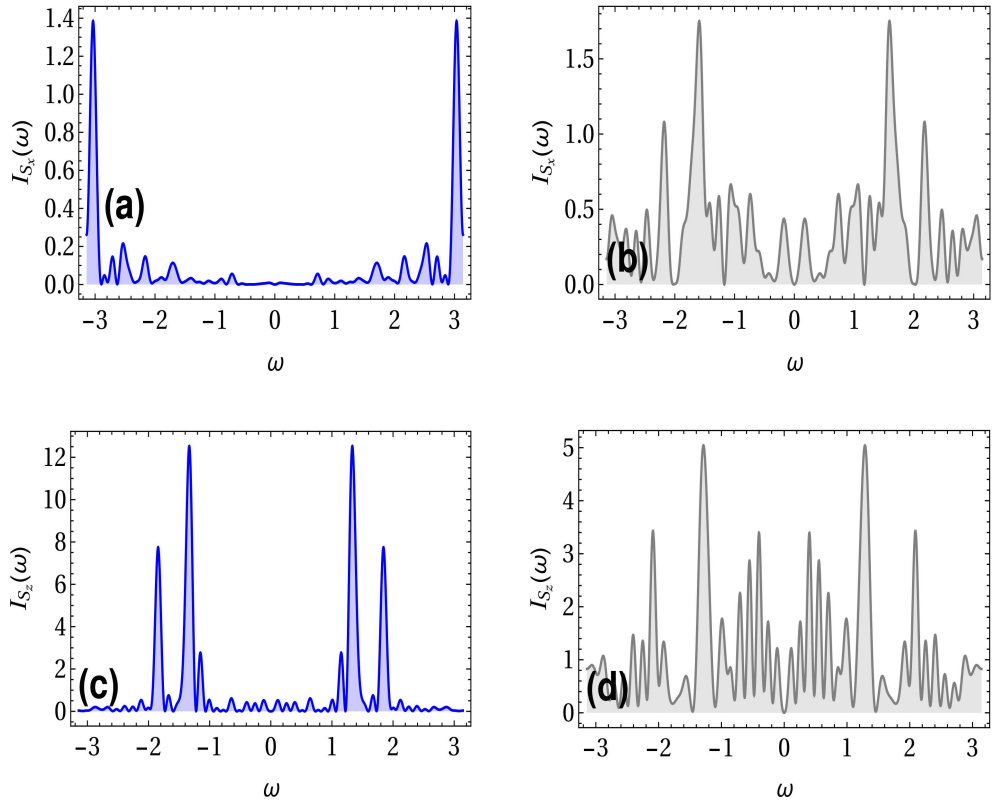

Fig. 3.8 Fourier Power spectrum density for the components $S_{x,z}$ in the regular regime ((a) and (c)) at $K = 0.5$ (Blue), and in the chaotic regime ((b) and (d)) at $K = 10$ (Gray). The parameters used for the plot are $m = 1$, $g = 1$, $\Omega = 1$, $\delta = 1$, $\omega_r = 0.2$, $T = 1$, $\alpha = \pi/2$. The values of the parameters in the real units: $K = \varepsilon I_0 T \frac{6\pi\mu}{m^2\omega_r^2}$, $\mu = \frac{\omega_r^2 m}{2a_0^2}$ $I_0 = \frac{m}{2}x_0^2\omega_r$, $m = 6\times10^{-17}$Kg, $x_0 = a_0 = 5\times10^{-3}$m, $T = 10\mu$s, $\omega_r = \omega_0 = 2\pi\times5\times10^6$Hz, for chaotic case $\varepsilon = 0.003$ and for the regular case $\varepsilon = 0.0003$.

to the analysis of spin-1/2 case discussed in Section 3.3, we calculate time-dependent wave function for the system Eq. (3.24) using $\delta_\pm = \delta$ and $\Omega_\pm = \Omega$ can be written as:

$$|\psi(t = NT)\rangle = \sum_{\{\alpha_n\}=1,2,3} \left\{ \prod_{n=2}^{N} e^{-i\alpha_n\varphi_n} \langle \varphi_n^{\alpha_n} | \varphi_{n-1}^{\alpha_{n-1}} \rangle \right\} e^{-i\alpha_1\varphi_1} \langle \varphi_1^{\alpha_1} | \psi(0) \rangle | \varphi_N^{\alpha_N} \rangle. \tag{3.25}$$

Here $\alpha_n\varphi_n$ and $|\varphi_n^{\alpha_n}\rangle$ ($\alpha_n = 1,2,3$) are the eigenvalues and eigenstates of the nth Floquet operator $\hat{\mathscr{F}}_n$, respectively. The spectral decomposition of $\hat{\mathscr{F}}_n$ is given as

$$\hat{\mathscr{F}}_n = \exp\{-i\varphi_n^1\}|\varphi_n^1\rangle\langle\varphi_n^1| + \exp\{-i\varphi_n^2\}|\varphi_n^2\rangle\langle\varphi_n^2| + \exp\{-i\varphi_n^3\}|\varphi_n^3\rangle\langle\varphi_n^3| \tag{3.26}$$

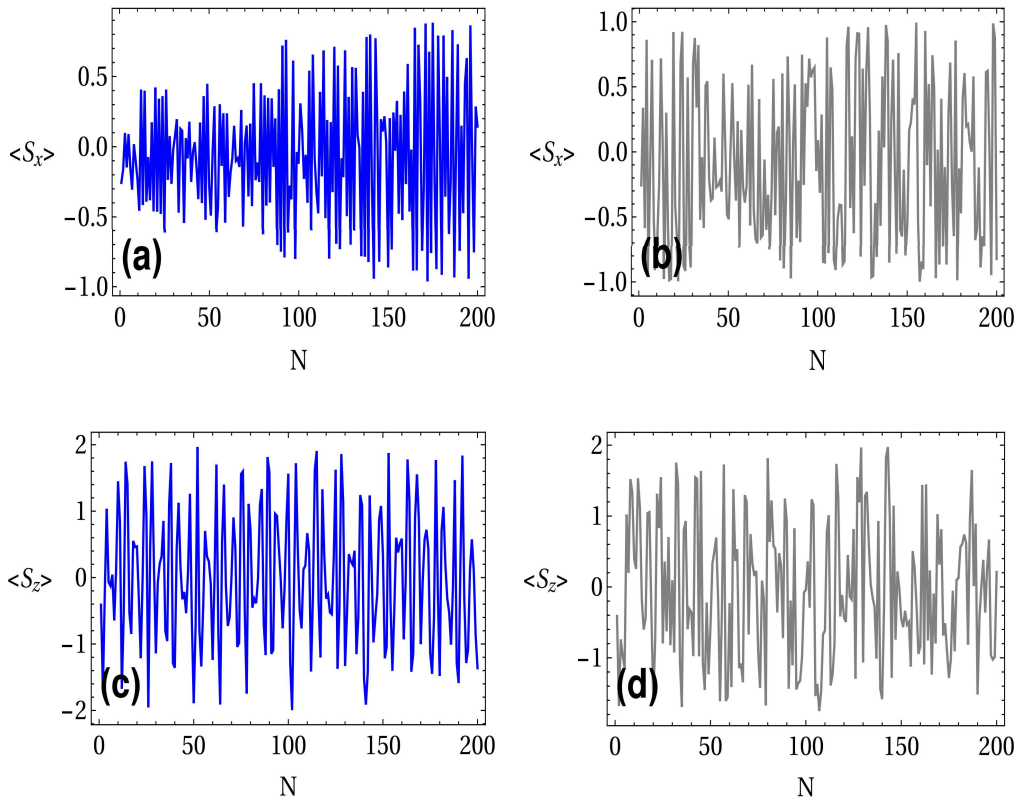

Fig. 3.9 Spin dynamics for the components S_x and S_z for Spin-1 case in the regular regime at $K = 0.5$ ((a) and (c)) and in the chaotic regime at $K = 10$ ((b) and (d)). The parameters are $m = 1$, $g = 1$, $\Omega = 1$, $\delta = 1$, $\omega_r = 0.2$, $T = 1$, $\alpha = \pi/2$. The values of the parameters in the real units: $K = \varepsilon I_0 T \frac{6\pi\mu}{m^2\omega_r^2}$, $\mu = \frac{\omega_r^2 m}{2a_0^2}$, $I_0 = \frac{m}{2}x_0^2\omega_r$, $m = 6\times10^{-17}$Kg, $x_0 = a_0 = 5\times10^{-3}$m, $T = 10\mu$s, $\omega_r = \omega_0 = 2\pi\times5\times10^6$Hz, for chaotic $\varepsilon = 0.003$ and for regular $\varepsilon = 0.0003$.

In the above equation, the quasienergy φ_n is given by $\varphi_n^{1,2,3} = \delta, \frac{1}{2}(-\delta \pm \sqrt{\delta^2 + (2\chi_n + \sqrt{2}\Omega)^2})T$, where the notation $\chi_n = g\sqrt{2I_n/m\omega_r}\cos\theta_n$ is already defined in section 3.3. In this case the normalized eigenstates are $|\varphi_n^1\rangle = -\eta_n|0\rangle + \xi_n|1\rangle + \zeta_n|2\rangle$, and $|\varphi_n^2\rangle = x_n|0\rangle + y_n|1\rangle + z_n|2\rangle$and $|\varphi_n^3\rangle = u_n|0\rangle + v_n|1\rangle + w_n|2\rangle$. The normalization constants of the eigenstates are defined in Appendix B . S-V.

We prepare the system initially in the state $|\psi(0)\rangle = |0\rangle$. The explicit form of the evolved wave function from Eq. (3.25) takes the form

$$
\begin{aligned}
&|\psi(t=NT)\rangle = \mathscr{A}_{11}\{-\eta_1 \exp(-i\varphi_1^1)(-\eta_N|0\rangle + \xi_N|1\rangle + \eta_N|2\rangle)\} \\
&+\mathscr{A}_{12}\{-\eta_1 \exp(-i\varphi_1^1)(x_N|0\rangle + y_N|1\rangle + z_N|2\rangle)\} + \mathscr{A}_{13}\{-\eta_1 \exp(-i\varphi_1^1)(u_N|0\rangle \\
&+v_N|1\rangle + w_N|2\rangle)\} + \mathscr{A}_{21}\{x_1 \exp(i\varphi_1^2)(-\eta_N|0\rangle + \xi_N|1\rangle + \eta_N|2\rangle)\} \\
&+\mathscr{A}_{22}\{x_1 \exp(i\varphi_1^2)(x_N|0\rangle + y_N|1\rangle + z_N|2\rangle)\} + \mathscr{A}_{23}\{x_1 \exp(i\varphi_1^2)(u_N|0\rangle + v_N|1\rangle + w_N|2\rangle)\} \\
&+\mathscr{A}_{31}\{u_1 \exp(i\varphi_1^3)(-\eta_N|0\rangle + \xi_N|1\rangle + \eta_N|2\rangle)\} + \mathscr{A}_{32}\{u_1 \exp(i\varphi_1^3)(x_N|0\rangle + y_N|1\rangle + z_N|2\rangle)\} \\
&+\mathscr{A}_{33}\{u_1 \exp(i\varphi_1^3)(u_N|0\rangle + v_N|1\rangle + w_N|2\rangle)\}, \qquad (3.27)
\end{aligned}
$$

where the coefficients A_{ij} are calculated from

$$
\begin{aligned}
\mathscr{A} &= \prod_{n=2}^{N} G_n\{\varphi\}, \\
G_n\{\varphi\} &= \begin{pmatrix} G_{11} & G_{12} & G_{13} \\ G_{21} & G_{22} & G_{23} \\ G_{31} & G_{32} & G_{33} \end{pmatrix}. \qquad (3.28)
\end{aligned}
$$

The matrix elements of Eq. (3.27) is defined in Appendix B . S-V.

Again, for spin-1 case we study spin dynamics and analyze the Fourier power spectrum of operators defined as follows $I_{S_x,S_y,S_z} = \left| \int_{-\infty}^{\infty} \langle S_{x,y,z} \rangle \exp(-i\omega t) dt \right|^2$, where $S_{x,y,z}$ are spin components for $S = 1$ case. The Fourier power spectrum for S_x and S_z components are plotted in Figs. 3.8 for the regular $K = 0.5$ and chaotic $K = 10$ regimes. We clearly see from Figs. 3.8 that in the regular regime we get a few sharp peaks but in the chaotic regime we see broadening of the spectrum and many peaks which is a signature of chaos. The continuously filled lower band manifests the essence of the chaos in the spin dynamics. Spin dynamics for S_x and S_z components for regular and chaotic cases are plotted in Figs. 3.9 (a)-(d). The spin dynamics clearly differentiates between regular and chaotic

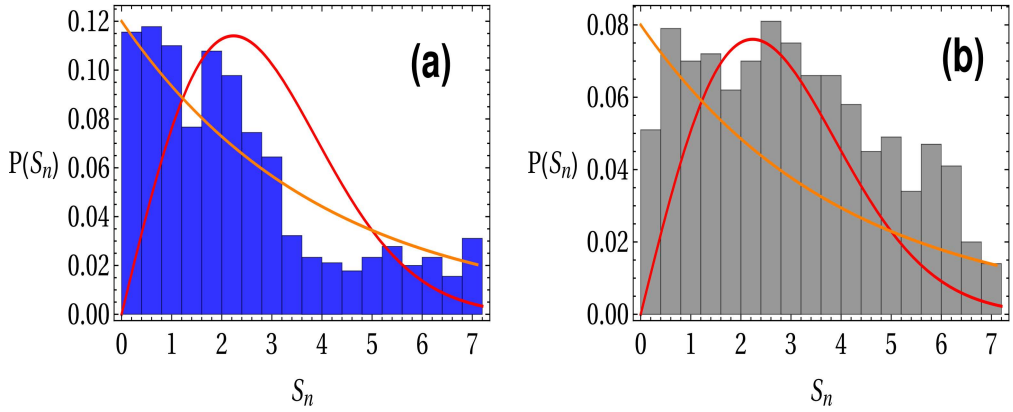

Fig. 3.10 Histogram plot of level statistics of Hamiltonian $\hat{H}_n = \hat{H}_{NV} + g\hat{V}_{c,NV}$ for spin-1 system (a) in the regular regime at $K = 0.5$ (Blue) and (b) in the chaotic regime $K = 10$ (Gray). A reference plot for Poissonian statistics (Orange) and Gaussian statistics (Red) is also shown. 1000 kicks are considered. The parameters are $m = 1$, $g = 1$, $\Omega = 1$, $\delta = 1$, $\omega_r = 0.2$, T=1, $\alpha = \pi/2$. The values of parameters: $K = \varepsilon I_0 T \frac{6\pi\mu}{m^2\omega_0^2}$, $\mu = \frac{\omega_r^2 m}{2a_0^2}$ $I_0 = \frac{m}{2}x_0^2\omega_r$, $m = 6\times10^{-17}$Kg, $x_0 = a_0 = 5\times10^{-3}$m, T=10$\mu$s, $\omega_r = \omega_0 = 2\pi\times5\times10^6$Hz, for chaotic case $\varepsilon = 0.003$ and for the regular case $\varepsilon = 0.0003$.

case. A quasi periodic oscillation is visible when the oscillator is in the regular regime and a chaotic oscillation for the oscillator in the chaotic regime. Transition from the quasi periodic to the chaotic spin dynamics while changing the stochasticity parameter K from 0.5 to 10 is a signature of chaos. Following the recipes used for spin-1/2 case in section 3.3 we analyze the nearest-neighbour level statistics for spin-1 case. In the three-level system, two nearest-neighbour spacings at n^{th} kick are given as

$$\begin{aligned} S_n^1 &= E_2^{(n)} - E_3^{(n)} = \frac{1}{2}\big(-\delta + \sqrt{(2\chi_n + \sqrt{2}\Omega)^2 + \delta^2}\big), \\ S_n^2 &= E_1^{(n)} - E_2^{(n)} = \frac{1}{2}\big(\delta + \sqrt{(2\chi_n + \sqrt{2}\Omega)^2 + \delta^2}\big), \end{aligned} \tag{3.29}$$

We calculate the nearest-neighbour spacing for a few kicks and plot the distribution functions. For the calculation of level-spacing distribution of the Hamiltonians at different kicks, we notice that the off-diagonal entries of the Hamiltonians contain I_n and θ_n having range $[0, 2\pi]$ with ($mean \sim 3.132$ and $variance \sim 3.382$) are stochastic. In the chaotic case of $S = 1$, the distribution of the off-diagonal entries form a Gaussian ensemble with a

mean of 0.49 and a variance 5.7 and level-spacing distribution is not the same as that of Gaussian orthogonal ensemble [222] but the effect of level repulsion is visible in this larger Hilbert space which was absent in the spin-1/2. In Fig. 3.10 we show the level-spacing distribution of regular and chaotic regimes for $S = 1$ case with a reference Poissonian $P(S) \propto \exp(-S)$ and Wigner-Dyson distributions $P(S) \propto (\pi S/2)\exp(-\pi(S/2)^2)$. We see that the maxima of distribution functions $P(S_n)$ in the regular case are shifted to the area of small S_n and in the chaotic case to the finite S_n. Although distribution functions are not strictly Poissonian or Wigner-Dyson type, the effect of the level repulsion is attributed to the quantum chaotic phenomena is observed. Indeed increasing the spin size enhances the visibility of signature of quantum chaos but at the same time this would move the model away from the system of physical interest.

3.5 Statistical average over various I_0 and θ_0

One of the principle differences between classical and quantum chaos is the sensitivity of the classical nonlinear dynamics with respect to the slight change of the initial conditions. Typically chaotic classical phase trajectories diverge in time when starting from the vicinity of the same region. We want to know if classical chaos imposes certain effects on the quantum subsystem in the case of hybrid quantum-classical chaos. For this aim, we considered the statistical average over many initial values I_0 and θ_0.

Results of numeric calculations are presented in Figs. 3.11 and Figs. 3.12.

As we see from the plots, quantum dynamics is less sensitive to the averaging performed on the classical part. Chaotic $K > 1$ and regular $K < 1$ characteristics of quantum dynamics is preserved after averaging done over the classical cantilever.

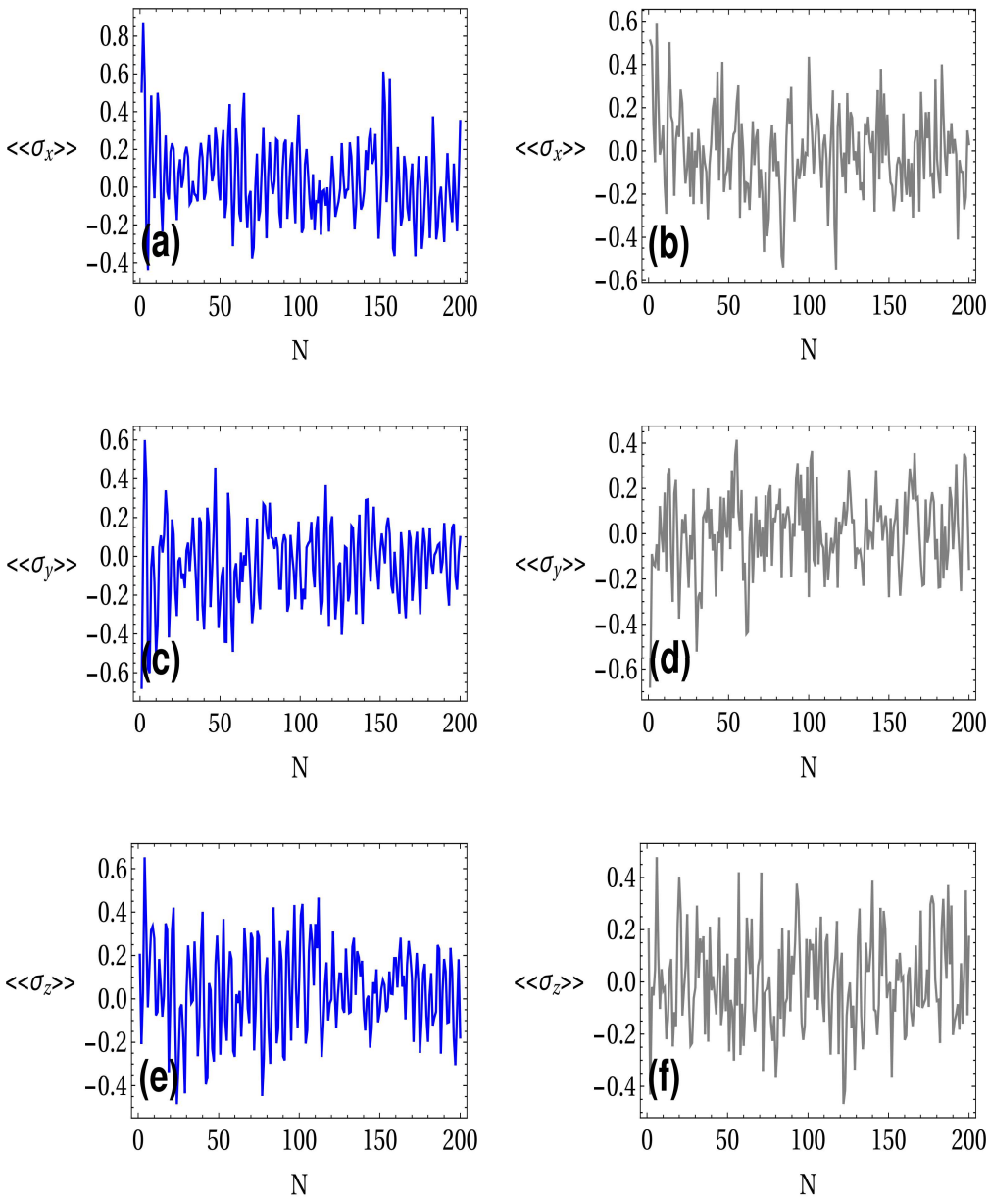

Fig. 3.11 Statistical average of spin dynamics (Spin-1/2 system) for $\langle\langle\sigma_x\rangle\rangle$, $\langle\langle\sigma_y\rangle\rangle$ and $\langle\langle\sigma_z\rangle\rangle$ in the regular regime at $K = 0.5$ ((a), (c) and (e)) and in the chaotic regime at $K = 10$ ((b), (d) and (f)). For calculating statistical average of spin dynamics (Spin-1/2 system) we have taken 15 different sets of (I_0, θ_0). The parameters are $m = 1$, $g = 1$, $\omega_0 = 1$, $\omega_r = 0.2$, $T = 1$, $\alpha = \pi/2$. The values of the parameters in the real units: $K = \varepsilon I_0 T \frac{6\pi\mu}{m^2\omega_r^2}$, $\mu = \frac{\omega_r^2 m}{2a_0^2}$, $I_0 = \frac{m}{2}x_0^2\omega_r$, $m = 6\times10^{-17}$Kg, $x_0 = a_0 = 5\times10^{-3}$m, $T = 10\mu$s, $\omega_r = \omega_0 = 2\pi\times5\times10^6$Hz, for chaotic $\varepsilon = 0.003$ and for regular $\varepsilon = 0.0003$.

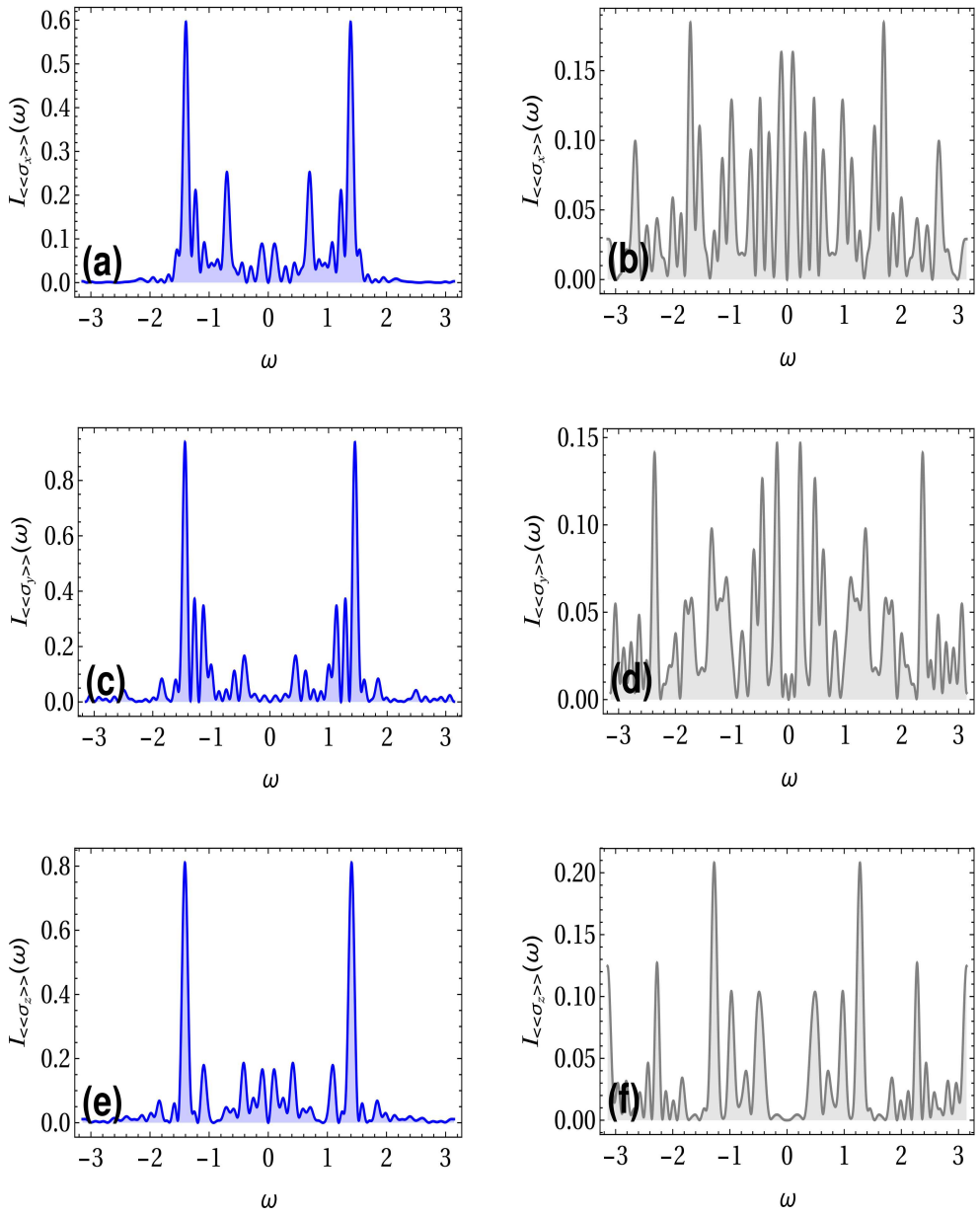

Fig. 3.12 Statistical average of Fourier Power spectrum density (Spin-1/2 system) for $\langle\langle\sigma_x\rangle\rangle$, $\langle\langle\sigma_y\rangle\rangle$ and $\langle\langle\sigma_z\rangle\rangle$ in the regular regime ((a), (c) and (e)) at $K = 0.5$ (Blue), and in the chaotic regime ((b), (d) and (f)) at $K = 10$ (Gray). For calculating Statistical average of Spin dynamics(Spin-1/2 system) we have taken 15 different sets of (I_0, θ_0). The parameters used for the plot are $m = 1$, $g = 1$, $\omega_0 = 1$, $\omega_r = 0.2$, $T = 1$, $\alpha = \pi/2$. The values of the parameters in the real units: $K = \varepsilon I_0 T \frac{6\pi\mu}{m^2\omega_r^2}$, $\mu = \frac{\omega_r^2 m}{2a_0^2}$ $I_0 = \frac{m}{2}x_0^2\omega_r$, $m = 6\times10^{-17}$Kg, $x_0 = a_0 = 5\times10^{-3}$m, $T = 10\mu$s, $\omega_r = \omega_0 = 2\pi\times5\times10^6$Hz, for chaotic case $\varepsilon = 0.003$ and for the regular case $\varepsilon = 0.0003$.

3.6 Feedback Effect

An interesting question is the feedback of the quantum subsystem on the classical dynamics. For studying this problem one needs to solve recurrent relations self-consistently together with the Schrödinger equation. After transforming into the action-angle variables we deduce:

$$\begin{aligned}
&\frac{d|\psi\rangle}{dt} = -\frac{i}{\hbar}\left(\hat{H}_s + g\sqrt{2I/m\omega_r}\cos\theta\hat{S}_z\right)|\psi\rangle, \\
&\frac{dI}{dt} = -\frac{\partial H_{I,\theta}}{\partial\theta} - \frac{\partial\hat{V}_{c,NV}}{\partial\theta} = g\sqrt{2I/m\omega_r}\sin\theta\langle\psi|\hat{S}_z|\psi\rangle \\
&-\varepsilon\frac{\partial V(I,\theta)}{\partial\theta}T\sum_{n=-\infty}^{\infty}\delta(t-nT), \\
&\frac{d\theta}{dt} = \frac{\partial H_{I,\theta}}{\partial I} - \frac{\partial\hat{V}_{c,NV}}{\partial I} = -\frac{g}{\sqrt{2m\omega_r I}}\cos\theta\langle\psi|\hat{S}_z|\psi\rangle + \omega(I) + \\
&\varepsilon\frac{\partial V(I,\theta)}{\partial I}T\sum_{n=-\infty}^{\infty}\delta(t-nT).
\end{aligned} \tag{3.30}$$

The standard procedure for solving Eq.(3.30) consists of two steps: free propagation and kick. During the free propagation, the effect of kicks is absent and vice versa. We note that our system is inherently nonlinear, and nonlinearity is a part of the main Hamiltonian. The nonlinearity in our case is not weak, and the model is non-perturbative. While action I is an adiabatic variable, angle θ is a fast oscillating variable such that $T\theta > 2\pi$. The formal solution of the recurrent relations has a form of morphism $\mathscr{M} = I_n, \theta_n \to I_{n+1}, \theta_{n+1}$, where $n, n+1$ corresponds to the values after nth and $(n+1)^{\text{th}}$ kick, respectively. We have two time scales in the problem, fast and slow. The time unit for the evolution of I and θ is T. Meaning that on the times shorter than $t < T$ variables I_n, θ_n are constants. To go from I_n, θ_n to I_{n+1}, θ_{n+1} we need at least time $t = T$. On the other hand we have fast time oscillations in the Schrödinger equation because $\omega_0 \gg g$. However, these fast phase

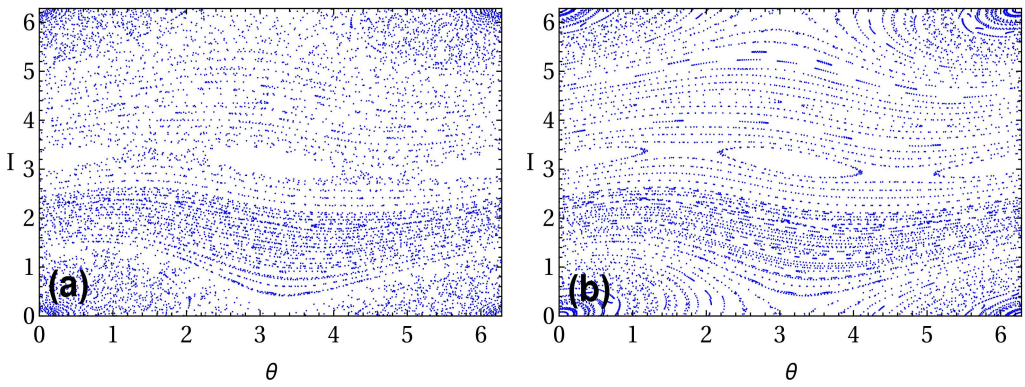

Fig. 3.13 The Phase space plot of cantilever's dynamics constructed through the recurrence relations Eq. (3.37) with feedback in ((a) and (b)) the regular regime $K = 0.5$ (Blue) where the phase space is covered by two different phase trajectories: open hyperbolic and some part of closed ellipse.The parameters for fig.3.13(a) are $m = 1$, $g = 0.1$, $\omega_0 = 10$, $\omega_r = 0.2$, $T = 1$. The parameters for fig.3.13(b) are $m = 1$, $g = 0.01$, $\omega_0 = 1$, $\omega_r = 0.2$, $T = 1$. The values of the parameters in the real units: $K = \varepsilon I_0 T \frac{6\pi\mu}{m^2\omega_r^2}$, $\mu = \frac{\omega_r^2 m}{2a_0^2}$ $I_0 = \frac{m}{2}x_0^2\omega_r$, $m = 6\times10^{-17}$Kg, $x_0 = a_0 = 5\times10^{-3}$m, $T = 10\mu$s, $\omega_r = \omega_0 = 2\pi\times5\times10^6$Hz, for the regular case $\varepsilon = 0.0003$.

oscillations of the wave function are distinct from the evolution of the wave function that occurs on the larger time scale $t > T$ due to the evolution of I_n, θ_n. Existence of fast and slow time scales in the system allows us to tackle the feedback problem in the following scheme: In order to obtain fast time evolution of the wave function valid for $t < T$, we solve the first equation in Eq.(3.30) for a constant I_n, θ_n (for $t < T$, variables I_n and θ_n are constant). We solve Schrödinger equation analytically:

$$\frac{d|\psi\rangle}{dt} = -\frac{i}{\hbar}\left(\hat{H}_s + g\sqrt{2I/m\omega_r}\cos\theta\hat{S}_z\right)|\psi\rangle, \tag{3.31}$$

where $\hat{S}_z = \frac{1}{2}(\cos\alpha\sigma_z + \sin\alpha(\sigma^+ + \sigma^-))$. When I_n and θ_n are constants, $a_n = \sqrt{2I_n/m\omega_r}\cos\theta_n = V_0(I_n)\cos\theta_n$ is also a constant.

After solving Schrödinger's equation analytically, we get the evolved wave function as:

$$|\psi\rangle = \begin{pmatrix}\Xi_1\\ \Xi_2\end{pmatrix}, \tag{3.32}$$

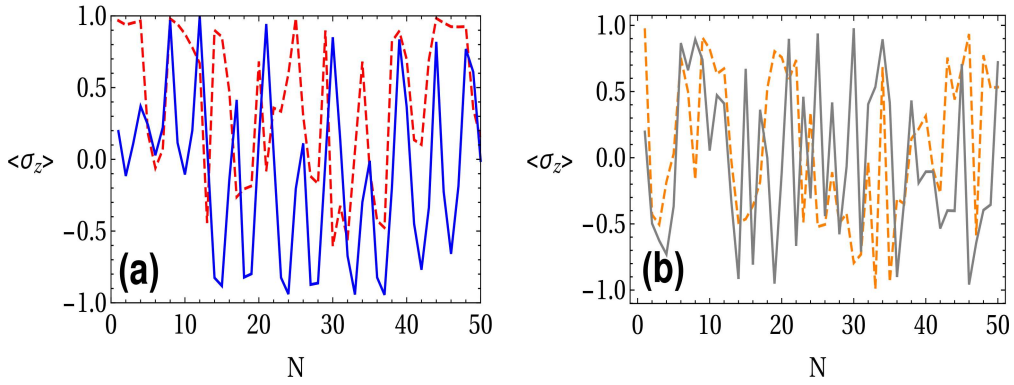

Fig. 3.14 Spin dynamics with feedback (Solid) and without feedback (Dashed) for $\langle\sigma_z\rangle$ in the regular regime at $K = 0.5$ (see (a)) and $\langle\sigma_z\rangle$ in the chaotic regime at $K = 10$ (see (b)). The parameters are $m = 1$, $g = 1$, $\omega_0 = 1$, $\omega_r = 0.2$, $T = 1$, $\alpha = \pi/2$. The values of the parameters in the real units: $K = \varepsilon I_0 T \frac{6\pi\mu}{m^2\omega_r^2}$, $\mu = \frac{\omega_r^2 m}{2a_0^2}$, $I_0 = \frac{m}{2}x_0^2\omega_r$, $m = 6\times10^{-17}$Kg, $x_0 = a_0 = 5\times10^{-3}$m, $T = 10\mu$s, $\omega_r = \omega_0 = 2\pi\times5\times10^6$Hz, for chaotic $\varepsilon = 0.003$ and for regular $\varepsilon = 0.0003$.

where

$$\Xi_1 = \frac{-ia_n g \sin\frac{1}{2}t\sqrt{a_n^2g^2+\omega_0^2}}{\sqrt{a_n^2g^2+\omega_0^2}}, \tag{3.33}$$

and

$$\Xi_2 = \cos\frac{1}{2}t\sqrt{a_n^2g^2+\omega_0^2} + \frac{i\omega_0\sin\frac{1}{2}t\sqrt{a_n^2g^2+\omega_0^2}}{\sqrt{a_n^2g^2+\omega_0^2}}. \tag{3.34}$$

Here we introduced shorthand notation $\Omega_n = \sqrt{a_n^2g^2+\omega_0^2}$. We note that ω_0 is a large parameter of the proposed theoretical model and this assumption is based on the value of $\omega_0 = 2.88$GHz for NV centres. Therefore $\omega_0 \gg a_n g$ and $\sqrt{a_n^2g^2+\omega_0^2} \approx \omega_0$. To obtain the feedback term in the explicit form we calculate $\langle\psi(t)|\hat{S}_z|\psi(t)\rangle$ and deduce:

$$\int_0^T \langle\psi(t)|\hat{S}_z|\psi(t)\rangle dt = \frac{-a_n g\omega_0 T}{2\Omega_n^2} = \frac{-V_0(I_n)\cos\theta_n g T}{2\omega_0}. \tag{3.35}$$

Consequently Eq.(3.30) takes the form:

$$I_{n+1} = I_n + g\sqrt{2I_n/m\omega_r}\sin\theta_n \int_0^T \langle\psi(t)|\hat{S}_z|\psi(t)\rangle dt - K\sin\theta,$$
$$\theta_{n+1} = \theta_n + I_{n+1} - g\frac{\cos\theta_n}{\sqrt{2m\omega_r I_n}} \int_0^T \langle\psi(t)|\hat{S}_z|\psi(t)\rangle dt. \tag{3.36}$$

The explicit integrated feedback term Eq.(3.35) is plugged in the Eq.(3.36) and the generalized standard map is deduced in the form:

$$I_{n+1} = I_n - \frac{g^2 T V_0^2(I_n)}{4\omega_0}\sin 2\theta_n - K\sin\theta,$$
$$\theta_{n+1} = \theta_n + I_{n+1} + g^2 T\frac{\cos^2\theta_n}{2m\omega_r\omega_0}. \tag{3.37}$$

In Fig. 3.13 dynamics of cantilever with feedback effects in regular regime for $K = 0.5$ is shown. We see two cases: $g = 0.1$ and $g = 0.01$. When the interaction strength between NV spin and cantilever is moderate ($g = 0.1$), we see in Fig. 3.13(a) a small deviation from regular dynamics in presence of feedback. For small interaction between NV spin and cantilever, as shown in Fig. 3.13(b), feedback does not effect the dynamics of cantilever. In Fig. 3.14, we compare the spin dynamics with and without feedback effects. We see a minor change in the amplitude of oscillations in regular and chaotic cases due to the feedback term. In case of the regular regime, the feedback not much affect the magnetization as compared to the dynamics without feedback term. Similarly, the switching pattern is hardly affected in the chaotic regime.

3.7 Conclusions

In the present work, we studied hybrid quantum-classical NEMS systems. The classical part comprised of a nanocantilever, and the quantum part is the NV spin. Nanocantilever

performs nonlinear oscillations in the chaotic and regular regimes. Due to the spin-cantilever coupling, the effects of the oscillations of the cantilever are transmitted to the spin dynamics. The problem in question was whether the classical dynamical chaos may induce quantum chaos or other effects of quantum stochasticity in the quantum dynamics of the NV spin. We studied the Poincaré section of spin-dynamics and explored the Fourier power spectral density of the quantum dynamical observables in the chaotic and regular regimes. We investigated the generation of quantum coherence for the NV center coupled to nanocantilever in the chaotic and regular regime. We also investigated the quantum Poincaré recurrence in the chaotic and regular regime. While the Fourier spectrum analysis clearly indicates the presence of stochasticity in the dynamics of quantum observables, some characteristics of quantum chaos are absent. The dynamical chaos imposed to the cantilever dynamics through the kicking induces the stochastic dynamics on the quantum subsystem. However, this stochastic dynamics of the classical cantilever does not manifest all the features of quantum chaos. We also investigated a three-level system for the quantum part considering NV spin as spin-1 particle. We see that the Fourier power spectrum and spin dynamics evince the effects of chaos. For spin-1 case we see a quasi-Gaussian distribution of nearest-neighbour level spacing for the oscillator in chaotic regime and quasi-Poissonian level statistics for the oscillator in regular regime. We also explore the effect of quantum feedback on classical cantilever in both cases regular and chaotic and also see the effect on spin dynamics. Feedback effect is negligible in the chaotic regime of the system.